Interlocking characteristic and its correlation with interlayer shear strength in typical double-layered asphalt systems

Hongzhi He[a,b], Ali Rahman[a,b,c], Changfa Ai*[a,b]

[a] School of Civil Engineering, Southwest Jiaotong University, Chengdu, Sichuan 610031, China

[b] Key Laboratory for Highway Engineering of Sichuan Province, Southwest Jiaotong University, Chengdu, Sichuan 610031, China

[c] School of Civil Engineering, Faculty of Engineering and Physical Sciences, University of Leeds, Leeds, UK.

Abstract: Interlayer bonding condition is of great significance for maintaining the structural integrity of asphalt pavement structures. Addressing a crucial research gap, this study uniquely investigated the impact of interface morphology on interlocking properties and interlayer shear strength in three typical double-layered asphalt systems: AC-13/AC-20, SMA-13/AC-20, and OGFC-13/AC-20. Through the innovative application of nondestructive separation technology and three-dimensional (3D) laser scanning, interface morphology characteristics were thoroughly analyzed. This approach enabled the detailed extraction of texture parameters, unveiling the complex relationship between interface morphology and interlayer bonding strength. Interface shear tests further assessed the difference in shear strength, revealing significant differences in texture characteristics influenced by the mineral size variance in the upper layer. This analysis led to the development of a predictive model for interlayer shear strength based on morphological characteristics, offering a new tool for approximating the shear bonding condition, despite challenges in capturing the complex interaction between interface morphology and interlocking effects. The comprehensive examination of 3D interface morphology, combined with the shear strength analysis, clarified the mechanisms of interlayer bonding in relation to interface morphology. This breakthrough provides essential insights into the role of interface morphology in bonding efficacy and represents a significant advancement in understanding of interlayer bonding mechanisms.

Keywords: asphalt pavement; interface morphology; interlocking; interlayer shear strength; correlation.

1 Introduction

The quality of interlayer bonding is a key factor in determining the integrity of pavement structures. This quality is influenced by a multitude of factors, including the type and dosage of bonding materials, the impact of traffic load, variations in ambient temperature, interlayer contamination, as well as climatic conditions and the specifics of the construction process (Ghabchi and Dharmarathna 2020, Correia and Mugayar 2021, Raab 2011, Hristov 2018, Canestrari F 2013, Wruck et al. 2022). In asphalt pavements, the physical contact between upper and lower layers emerges as a pivotal component. An increasing body of research now directs attention towards the pavement structure integration, advocating for the enhancement of interlayer bonding through the lens of macromorphological contact (Chen et al. 2022, Liu et al. 2018, Somé et al. 2020).

Extensive research underscores the critical role of interface morphology in influencing interlayer bonding performance within pavement structures (Ktari et al. 2017, Hwang et al. 2022, Zhao et al. 2017, D'Andrea et al. 2013). Enhancements in interlayer bonding, achieved through the contribution of interlocking effects, have been substantiated in various practical applications. For instance, Ren et al. (2018), through the innovative technique of chip-sprinkling, which involves the application of stones to substructure surfaces, demonstrated that a textured interface significantly improves the shear durability of pavement structures, with residual shear strength achieving up to 80% of the interlayer's ultimate shear strength. Similarly, Liu et al. (2017) and Jaskula et al. (2021) observed that by inducing roughness on the lower layer surface through methods such as slotting, chiseling, and milling, the interlayer shear strength can be markedly enhanced. Further contributing to this body of work, Liao et al. (2016) showed that the strategic embedding of steel nails within the interlayer serves to efficiently distribute shear stresses between asphalt pavement layers. In addition, a number of studies were explored the efficacy of geosynthetic interlayers as reinforcement in asphalt layers (Ram Kumar B A V 2022, Solatiyan et al. 2021). These measures, aimed at altering interface contact morphology, have yielded significant improvements in interlayer bonding performance, showcasing the potential of such methodologies in enhancing the durability and longevity of pavement systems.

Most of the existing research adopts a macro-phenomenological perspective, often overlooking the interplay between interface morphology and interlayer bonding strength from a micro-morphological standpoint. Consequently, the mechanisms underpinning interlayer bonding, particularly in relation to the morphology of interlayer surfaces, remain insufficiently explored. Given the dual-surface nature of interlayers, a comprehensive understanding of the morphological characteristics of both upper and lower interlayer surfaces is imperative. Such an in-depth analysis is crucial not only for explaining interlocking effects but also for uncovering the fundamental relationship between interface morphology and interlayer bonding strength.

The significance of interface morphology on interlayer bonding has increasingly captivated the research community, with concerted efforts being made to identify the mechanisms driving its impact (White 2016). Tang et al. (2021) used an Olympus Microscope to capture the surface morphology of the lower layer, subsequently modeling it in three dimensions using MATLAB. Their findings indicated a positive correlation between surface roughness, shear strength, and variations in the tack coat rate. Similarly, Song et al. (2018) conducted a quantitative assessment of the interface contact area through image binarization techniques, revealing that a greater contact area and enhanced interlocking effect correspond to improved interlayer shear strength. The consensus among several studies is that a rich interface texture significantly increases the interlocking effect, thereby improving interlayer bonding within asphalt pavements (He et al. 2023, Tashman et al. 2008, Song et al. 2015, Song et al. 2017). Further contributing to this body of knowledge, Raab et al. (2012) utilized steel balls of varying sizes as model materials to thoroughly investigate the influence of material size on interlocking and interlayer shear strength. Their research clarified that optimal interlocking occurs when the upper layer material is smaller in size compared to the lower layer, underscoring the interplay between material size and interlayer bonding efficacy.

The evolution of measurement technologies, particularly non-contact scanning techniques, has significantly advanced pavement morphology research. This advancement has been pivotal in the domains of pavement texture analysis and road surface skid resistance, with notable contributions from (Jain et al. 2021, Medeiros Jr et al. 2021, Sha et al. 2020, Čelko et al. 2016, Kogbara et al. 2016). Among these innovations, Song et al. (2022) leveraged three-dimensional (3D) scanning to reconstruct interface morphology and assess interlayer fracture behavior, discovering that both the stress intensity factor (K_{IC}) and the critical strain energy release rate (J-integral) increased with the increase in texture depth (*TD*). Similarly, Mohamad et al. (2015) established a strong correlation between interface roughness of concrete and shear strength, leading to the development of a correlation model that integrates the roughness parameter with friction and cohesion coefficients. Furthermore, Hoła et al. (2015) utilized 3D laser scanning to derive morphological parameters of concrete interlayer surfaces, finding a significant linear relationship between the texture aspect ratio (*Str*) and peak material volume (*Vmp*). Despite these technological strides and empirical findings, a comprehensive understanding of how interface morphology influences interlayer bonding remains unknown.

The existing body of research on the morphology of layer interface in pavement structures remains incomplete, with the mechanisms of interlayer bonding in relation to interface morphology yet to be fully clarified. This gap underscores the need for a detailed exploration of interface morphology characteristics, their impact on the interlocking effect, and the subsequent influence on interlayer bonding strength. This study addresses these needs by reconstructing the 3D interface morphology of three bi-layered typical asphalt pavement structures. Utilizing advanced interlayer separation and 3D laser scanning technologies, detailed texture parameters were extracted to reveal these complex relationships.

In conjunction with analysis of interlayer shear strength test results, this study delves into the characteristics of interface morphology, the contribution of interlocking effect, and their collective impact on interlayer shear strength. Through an in-depth investigation, the complex interlayer bonding mechanism dictated by interface morphology was explained, offering novel insights into the underlying principles.

The findings of this research shed light on previously obscured aspects of the interlayer bonding mechanism, marking a significant step towards enhancing asphalt pavement structure integrity. By providing a fresh perspective and a detailed reference for understanding interlayer bonding, this study contributes valuably to the field, paving the way for advancements in interlayer bonding design. Figure 1 illustrates an overview of the methodology adopted in this study.

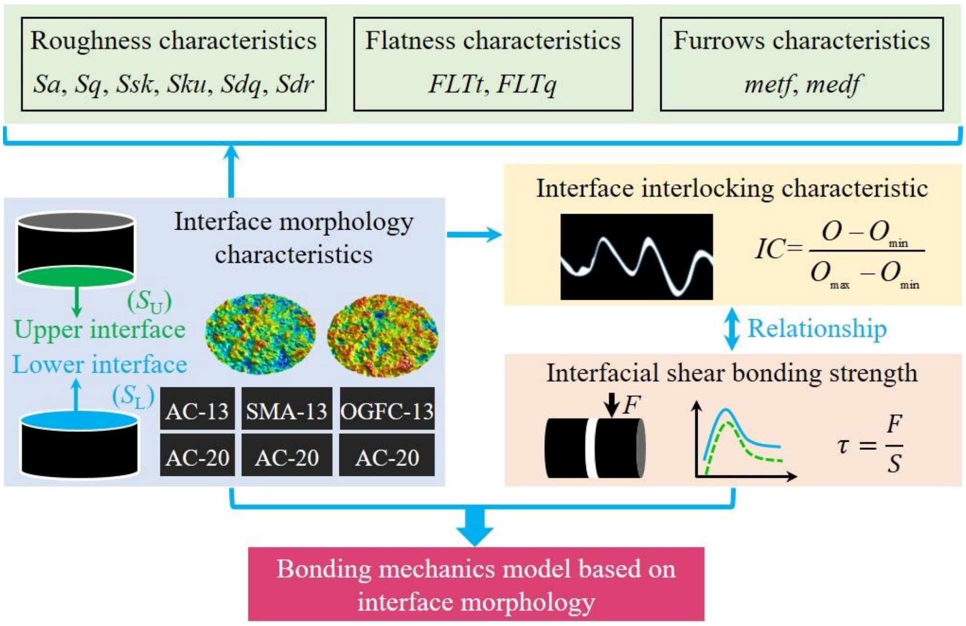

Figure 1. Overview of the proposed research plan.

2. Experimental program

2.1. Specimen preparation & non-destructive interface separation

In this study, three typical double-layered asphalt pavement structures were selected. Each of the three double-layered systems featured a uniform lower layer composed of dense-graded asphalt concrete (AC-20). Conversely, the composition of the upper layer differed in each structure: one utilized a dense-graded AC structure labeled as AC-13; another used a gap-graded stone mastic asphalt (SMA) structure, denoted as SMA-13; and the third incorporates an open-graded friction course (OGFC) structure, identified as OGFC-13. The aggregate gradation of each mixture was designed according to the Chinese Specification for Highway Asphalt Pavement Construction (JTG F40-2004) (China 2004), and the type of all mineral sizes in the mixtures are basalt. The gradation design and optimum asphalt content (OAC) of each mixture are shown in Table 1. The type of asphalt binder used in preparing each mixture was Styrene-Butadiene-Styrene (SBS)-modified asphalt while a modified emulsified asphalt, applied at a single application rate of 0.6 kg/m^2, was utilized as tack coat material. The properties of asphalt materials were determined according to the Chinese specification of "Highway Engineering Asphalt and Asphalt Mixture Test Procedure" (JTG E20–2011) (China 2011), as shown in Table 2.

Table 1. Gradation design and optimum asphalt content of asphalt mixtures.

Mix type	Passing rate of different sieve sizes in millimeter（%）												Optimum asphalt content (%)
	26.5	19	16	13.2	9.5	4.75	2.36	1.18	0.6	0.3	0.15	0.075	
AC-13	100	100	100	95	76.5	53	37	26.5	19	13.5	10	6	5.1
SMA-13	100	100	100	95	62.5	27	20.5	19	16	13	12	10	6.0
OGFC-13	100	100	100	95	70	21	16	12	9.5	7.5	5.5	4	4.4
AC-20	100	95	85	71	61	41	30	22.5	16	11	8.5	5	4.5

Table 2. Properties of SBS-modified and modified emulsified asphalt.

Material	Property		Test value	Specification limit	Test method (JTG E20)
SBS-modified asphalt	Penetration, 25 °C, 5 S, 100 g (0.1 mm)		55	40-60	T0604
	Ductility at 5°C (cm)		26	≥20	T0605
	Softening point (°C)		68	≥60	T0606
	Kinematic viscosity at 135°C (Pa·s)		1.79	≤3	T0620
	Flexible recovery at 25°C (%)		83	≥75	T0662
Emulsified asphalt	Particle charge		(+)	Cation (+)	T0653
	Sieve residue, 1.18 mm (%)		0.03	≤0.1	T0652
	Viscosity SFS at 25°C (Pa·s)		10	1~10	T0622
	Distillation residue	Residual content (%)	51	≥50	T0651
		Penetration at 25°C (0.1 mm)	60	40~120	T0604
		Ductility at 5°C (cm)	25	≥20	T0605

The process of specimen preparation using the Superpave gyratory compactor (SGC) is shown in Figure 2. A critical step involves the separation of layer interface within the bi-layered specimens. Extensive testing has confirmed the suitability of a silica gel isolation film for this purpose, owing to its softness and resistance to high temperatures. The optimal choice has been identified as an ultra-thin silica gel film, measuring 0.1 mm in thickness, which effectively facilitates the separation of the upper and lower interlayer surfaces. The procedural steps for this separation and subsequent interface acquisition were detailed in the previous study by the authors (Ai et al. 2022). Following is the summary of specimen preparation & non-destructive interface separation:

(1) The heated loose asphalt mixture was poured into a mold to form the lower layer with a diameter of 150 mm, which was then compacted to a height of 75 mm and left at room temperature to cool down for 24 hours.

(2) Half of tack coat material application rate, i.e. 0.3 kg/m^2, was applied on the clean surface of cooled lower layer, followed by the placement of an isolation film. Upon setting the film, the remaining half of the tack coat dosage was then applied over it, ensuring a uniform distribution. Subsequently, the coated surface was set aside at room temperature for 2 hours to allow the curing procedure to be completed.

(3) The loose asphalt mixture of upper layer was poured into the mold and compacted using a similar method applied in the first half of the mold.

(4) The fabricated bi-layered specimen was gently removed from the mold and allowed to condition at room temperature. This cooling period is critical to prevent damage to the asphalt specimen during the separation process.

(5) The final step involved delicately separating the upper and lower layers in a direction perpendicular to the interface plane, which are subsequently prepared for scanning.

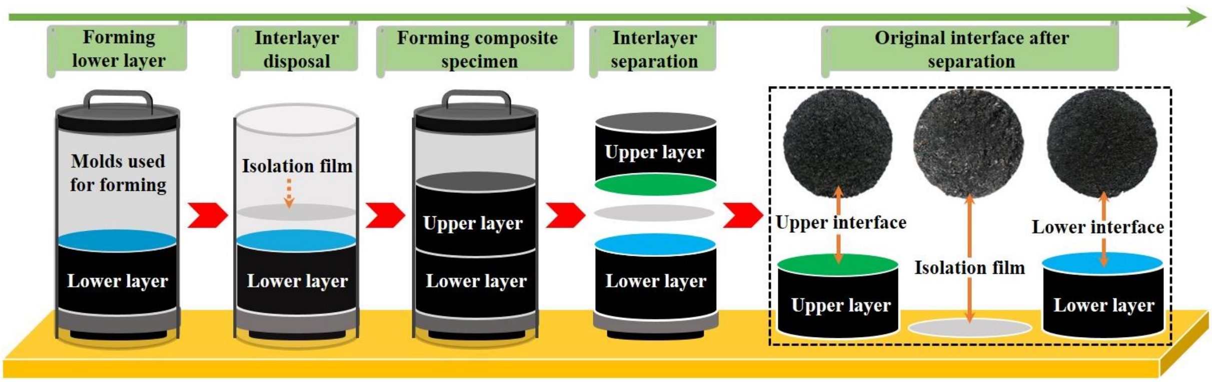

Figure 2. Preparation process of specimen to be scanned.

2.2. Interface 3D morphology

Following the separation of the layer interface, the morphology of interlayer surfaces was captured using a high-precision handheld 3D laser scanner, as depicted in Figure 3. For each pavement structure, scans were performed on three parallel specimens to ensure consistency and reliability of the data collected.

The point cloud data generated from these scans underwent a process of reconstruction using Geomagic Design X software, enabling the detailed rendering of the interfaces' 3D morphology.

Subsequent to reconstruction, the visualization of this 3D morphology was refined using MountainsMap® software, illustrated in Figure 4. This advanced software facilitated the calculation and extraction of critical morphological indices, providing a comprehensive dataset for analysis. This systematic approach to data acquisition and processing underscores the rigor of the methodology employed in capturing and analyzing the interface morphology within the studied pavement structures.

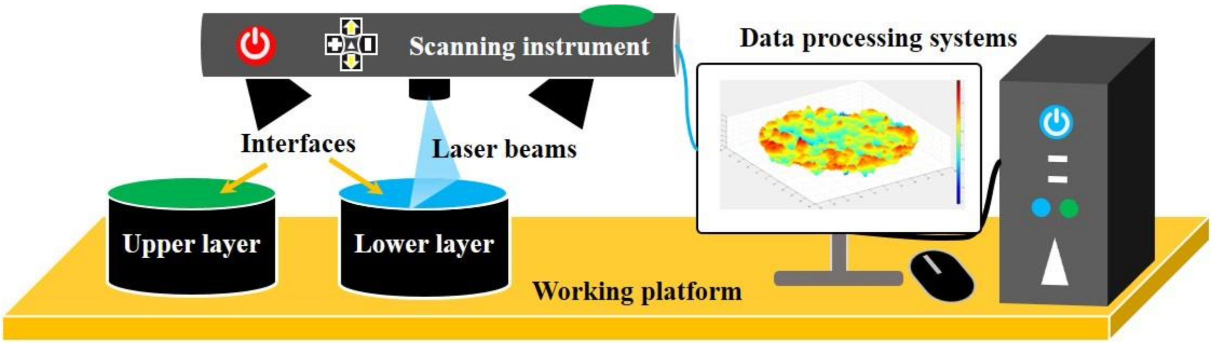

Figure 3. Schematic diagram of scanning of the layer interface.

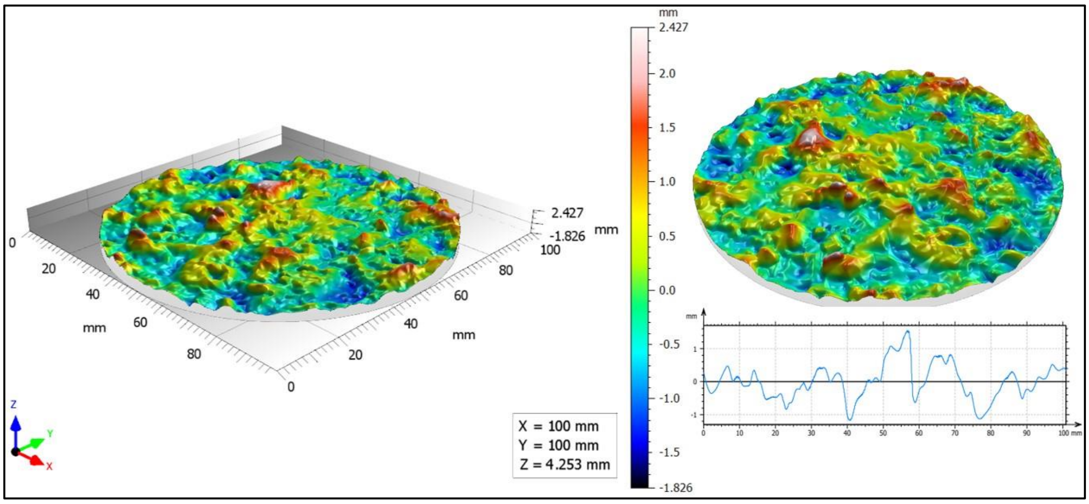

Figure 4. Data visualization, processing and index extraction of interface 3D morphology.

2.3. Interlayer bonding strength test

To assess the direct shear strength, the double-layered specimens were prepared in a similar method explained in Section 2.1. In the next step, specimens were organized into batches and subjected to a controlled environment, maintaining a steady temperature of 25°C for a duration of 4 hours. Subsequently, these conditioned specimens were mounted onto the direct shear testing apparatus. The application of shear load was facilitated through a universal testing machine (UTM), with the testing conducted at a constant shear rate of 50 mm/min (Goli et al. 2023, Han et al. 2021). Three replicates were considered for each group of specimens to ensure the reliability of the results obtained. A detailed schematic of the direct shear testing setup is provided in Figure 5.

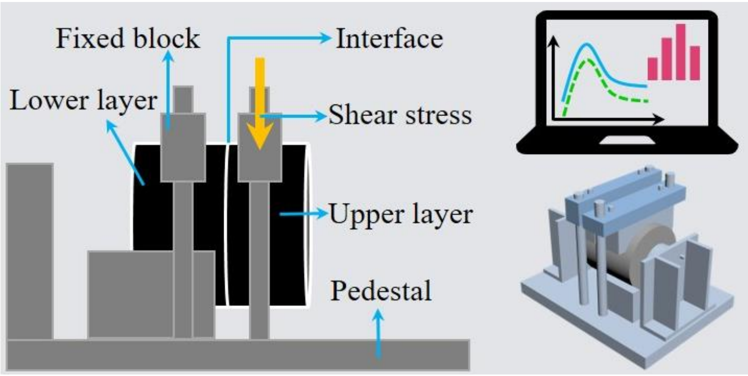

Figure 5. Schematic of direct shear test.

3. Methodology

To investigate the complex morphology and texture characteristics of the pavement interface, three primary characteristics of interface morphology were analyzed: roughness, flatness, and furrow characteristics. Detailed metrics for each of these morphological aspects, including their definitions, relevant standards, and units of measurement, are cataloged in Table 3.

Within this framework, *Sa*, *Sq*, *Ssk*, and *Sku* are indices that quantify the vertical aspects of surface texture. Conversely, *Sdq* and *Sdr* capture the composite texture parameters, reflecting the blend of height and spatial distribution of the surface features.

Figure 6 further visualizes these morphological indices, showcasing localized surface variations—both convex and concave—and their spatial distribution across the interface. This comprehensive approach allows for a deep understanding of the interface's morphology, laying the groundwork for correlating these characteristics with the interlayer bonding performance.

Table 3. List of interface morphological indicators.

Category	Index	Description	Standard	Unit	Literature
Roughness characteristic indexes	*Sa*	Arithmetic mean height	ISO 25178	mm	(Aver'yanova et al. 2017, Schulz et al. 2013)
	Sq	Standard deviation of the height distribution	ISO 25178	mm	
	Ssk	Skewness of the height distribution	ISO 25178	\	
	Sku	Kurtosis of the height distribution	ISO 25178	\	
	Sdq	Root mean square gradient	ISO 25178	\	
	Sdr	Developed interface area ratio	ISO 25178	%	
Flatness characteristic indexes	*FLTt*	Peak-to-valley flatness deviation	ISO 12781	mm	(Schulz et al. 2013, Nadolny K 2014)
	FLTq	Root mean square flatness deviation	ISO 12781	mm	
Furrow characteristics indicators	*metf*	Mean depth of furrows	Furrow	mm	(Schulz et al. 2013, Das et al. 2021)
	medf	Mean density of furrows	Furrow	cm/cm^2	

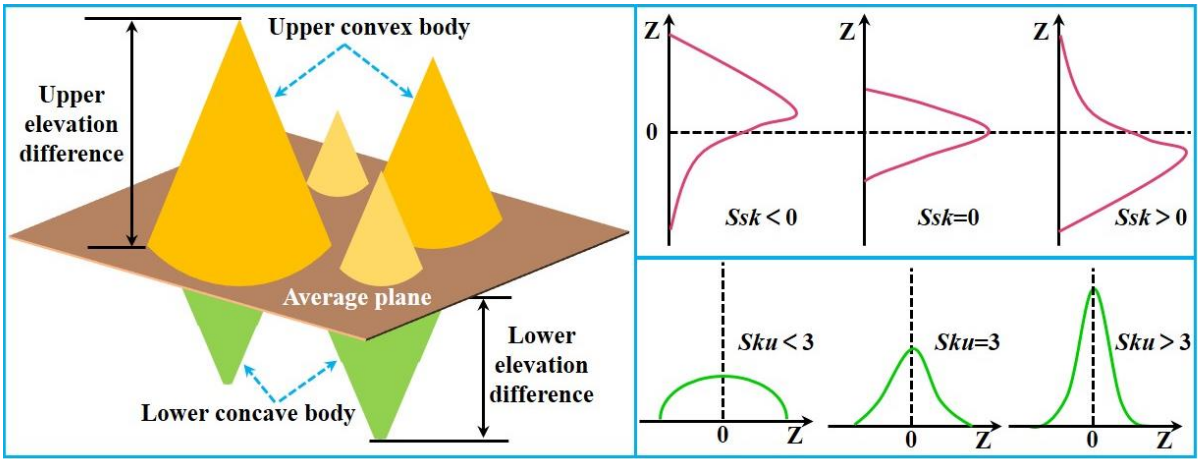

Figure 6. Localized surface convex and concave morphology and its distribution characteristics.

Sa quantifies the average absolute deviation of surface points from a mean plane, serving as an indicator of average surface roughness. *Sq* measures the standard deviation of heights across the surface points, reflecting the variability in surface elevation. *Ssk* assesses the symmetry of surface deviations. A value of *Ssk*=0 indicates a symmetrical distribution of peaks and valleys about the mean plane. *Ssk*<0 suggests a predominance of peaks above the mean surface, whereas *Ssk*>0 denotes a distribution skewed towards valleys below the mean surface. *Sku* complements *Ssk* by characterizing the peakedness of the height distribution. A *Sku* value of 3 corresponds to an ideal Gaussian distribution of surface heights. Values less than 3 imply a flatter, more dispersed distribution, whereas values greater than 3 indicate a sharper, more centralized distribution of surface elevations. *Sdq* calculates the root mean square gradient of the surface, with a value of 0 signifying a perfectly flat surface. As *Sdq* increases, so does the gradient, or slope, of the surface, highlighting the degree of surface incline. *Sdr* quantifies the relative increase in surface area due to textural features. Higher values of *Sdr* reflect greater texture amplitude and spacing, signifying a more pronounced surface texture.

FLTt is calculated as the sum of the absolute values of all deviations—both peaks and valleys—relative to a reference plane, typically determined by the least-squares method. This index offers a direct measure of the overall variance in surface height from the established norm, encapsulating the extremities of surface texture. *FLTq* represents the square root of the sum of the squares of the deviations of measurement points from the reference plane. This parameter specifically quantifies the aggregate deviation of the surface points, providing a holistic view of the surface's deviation from flatness.

Furthermore, are derived from the analysis of morphology profile lines and contour lines. *metf* quantifies the average depth of furrows, offering insights into the vertical aspects of the texture, while *medf* assesses the spatial frequency of these furrows across the surface, indicating how densely packed they are. These measurements are efficiently extracted using MountainsMap® software, allowing for a detailed exploration of the furrow features that contribute to the texture's complexity.

4 Results and discussion

4.1 Interlayer surface characteristics

4.1.1. Roughness Characteristics

The results of the statistical analysis regarding the interfaces roughness characteristics are depicted in Figure 7, with each subfigure dedicated to detailing the texture parameter statistics for both the upper and lower interlayer surfaces across the three evaluated double-layered asphalt systems. The following observations can be made:

(1) The analysis of the rough texture parameters, specifically *Sa* and *Sq*, across the upper and lower interlayer surfaces reveals a distinctive pattern among the three asphalt layer combinations studied. For both parameters, the OGFC-13/AC-20 structure exhibits the highest values, followed by SMA-13/AC-20, with AC-13/AC-20 showing the lowest values. Notably, the upper interlayer surfaces consistently register higher parameter values compared to their lower interface counterparts. This observation is attributed to the influence of the upper layer’s gradation on the interface roughness, given a uniform lower layer. The OGFC-13 structure, characterized by a skeletal void composition and a predominance of coarse aggregates, displays the greatest surface roughness. In contrast, the SMA-13 mixture, though also skeletal, is denser, and AC-13 features a continuous dense structure with a higher concentration of fine aggregates. Consequently, the roughness ranking, from most to least rough, aligns as OGFC-13, SMA-13, and AC-13. The interaction between the upper and lower layers plays a pivotal role in defining the interface's texture, with the lower surface (interface with AC-20) of the OGFC-13/AC-20 combination presenting the highest roughness, whereas the equivalent surface in the AC-13/AC-20 combination exhibits the least roughness.

(2) *Ssk* parameter manifests the degree of asymmetry in surface height distribution. For AC-13/AC-20 structure, both the upper and lower interlayer surfaces demonstrate a peak-like distribution, indicating a tendency towards positive skewness. In contrast, for OGFC-13/AC-20 and SMA-13/AC-20 structures, the upper interlayer surfaces exhibit a peak-like distribution, suggestive of protrusions, whereas their lower counterparts show a valley-like distribution, indicative of indentations. This phenomenon can be attributed to the presence of larger aggregates in OGFC-13 and SMA-13 mixes, which, upon embedding into the lower layer, create depressions that contribute to the valley-like distribution. Reflecting the sharpness or peakedness of the surface height distribution, the *Sku* parameter reveals that both upper and lower interlayer surfaces across all three asphalt structures register values greater than 3.

This denotes a pronounced sharpness in surface morphology, characterized by a peaked distribution that centers around a mean level. Among these, the interface of SMA-13/AC-20 structure is noted for its exceptional sharpness, suggesting a significant concentration of heights around a central peak compared to the other structures.

(3) The analysis of the *Sdq* parameter across the upper and lower interlayer surfaces of the three asphalt structures reveals that all values exceed 0, indicating the absence of completely flat interfaces. This observation suggests a universal presence of texture inclination across all examined surfaces. Notably, the variation in texture tilt across the lower interlayer surfaces of each structure is minimal, with significant differences primarily manifesting on the upper interlayer surfaces. The gradation of the upper layer's structure predominantly determines this variation, resulting in a texture roughness gradient that transitions from rough to flat in the sequence of OGFC-13, SMA-13, and AC-13. Further insights gained from the *Sdr* analysis illustrate that both the upper and lower interlayer surfaces exhibit an increase in area, with the upper surfaces demonstrating a higher area increase coefficient than their lower counterparts. This phenomenon underscores the pronounced texture characteristics of the OGFC-13/AC-20 interface, which exhibits the most significant texture differentiation, followed by SMA-13/AC-20 and AC-13/AC-20, in descending order of texture prominence.

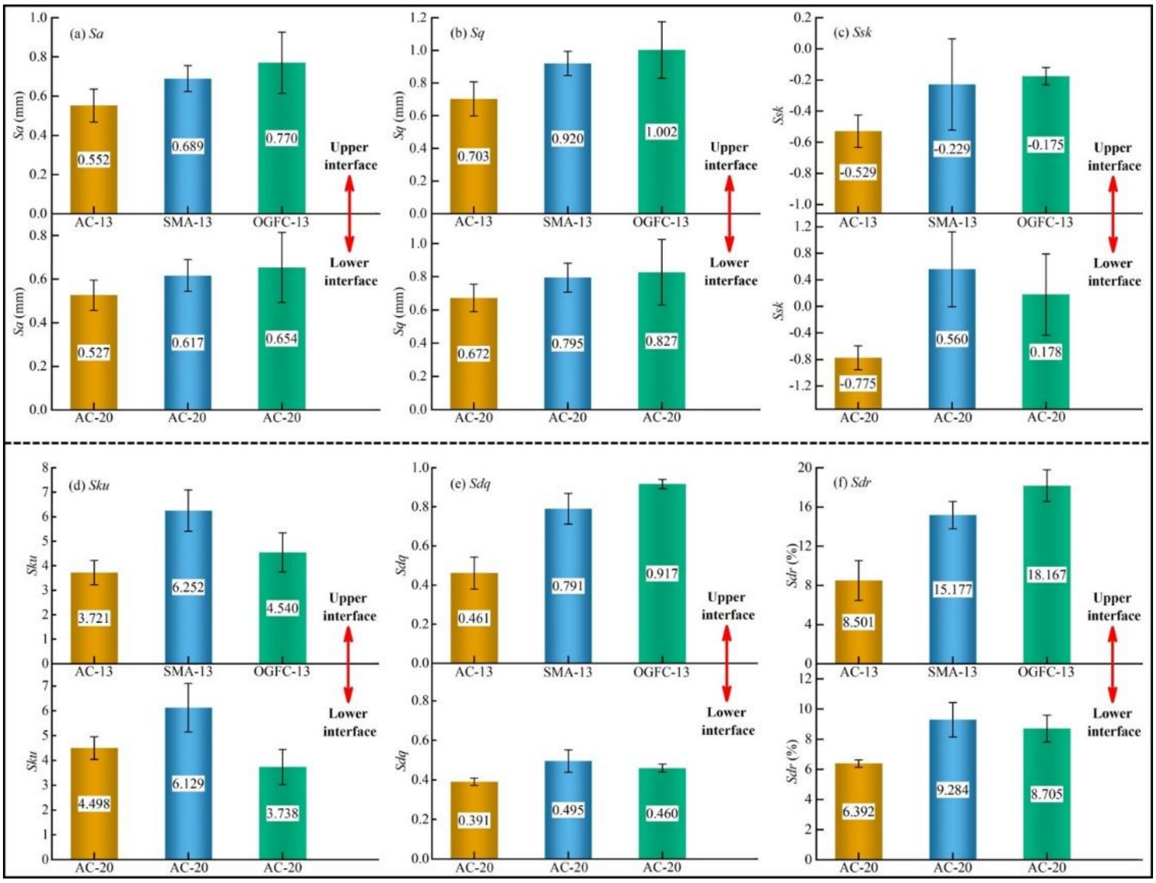

Figure 7. Results of roughness characteristics of interlayer of bi-layered asphalt structures.

4.1.2. Flatness Characteristics

As shown in Figure 8, the flatness metrics, including *FLTq* and *FLTt*, quantify the deviation of surface measurement points from a predefined reference plane. Among the evaluated interlayer surfaces, the OGFC-13/AC-20 combination displays the highest *FLTq* and *FLTt* values for its upper interlayer surface, indicating a pronounced deviation. Conversely, its lower surface presents the highest *FLTq* value, while the lower interlayer surface of SMA-13/AC-20 registers the highest *FLTt* value. In stark contrast, both the upper and lower surfaces of AC-13/AC-20 consistently show the lowest *FLTq* and *FLTt* values, denoting minimal deviation.

This analysis reveals that the flatness characteristics of OGFC-13/AC-20 and SMA-13/AC-20 share similarities, with each point deviating significantly from the reference plane, suggesting a rougher texture. The interlayer of AC-13/AC-20, conversely, exhibits relatively minor deviations, reflecting smoother surfaces. These differences are attributed to the gradational variations among the upper layer structures. The densely graded skeleton of AC-13/AC-20, characterized by a higher concentration of fine particles, contributes to a lesser degree of surface undulation, resulting in smoother interlayer interfaces.

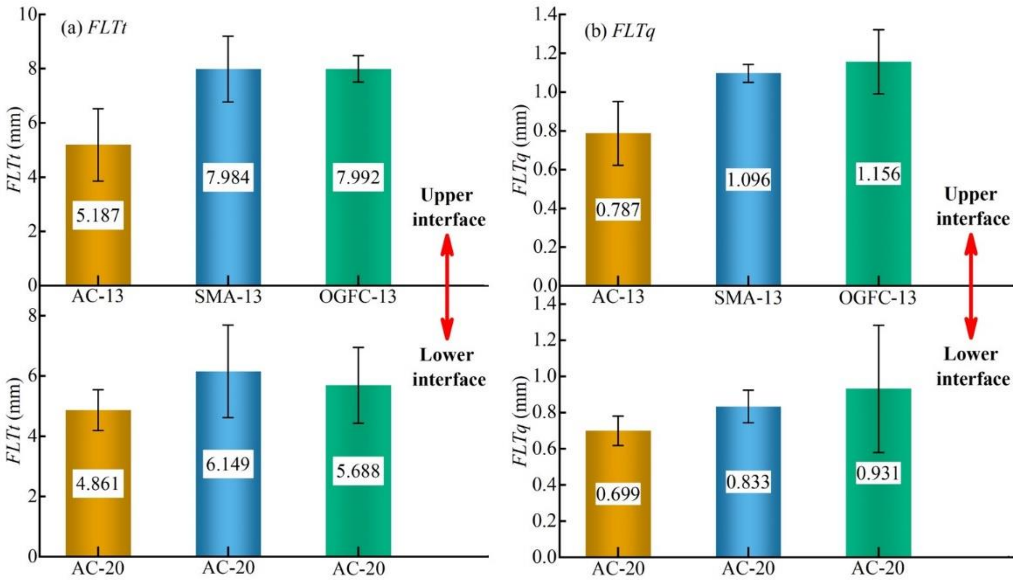

Figure 8. Results of flatness characteristics of interlayer of bi-layered asphalt structures.

4.1.3. Characteristics of furrow characteristics

Figure 9 clearly illustrates that the average furrow depths for both OGFC-13/AC-20 and SMA-13/AC-20 interfaces are notably similar and substantially exceed those observed for AC-13/AC-20. This observation corroborates earlier findings, highlighting that the presence of larger particles in the OGFC-13 and SMA-13 mixtures contributes to their pronounced interface texture characteristics. However, a contrasting trend is evident in the furrow density metrics, where OGFC-13/AC-20 and SMA-13/AC-20 exhibit lower densities compared to AC-13/AC-20. This difference is attributed to the densely graded nature of the AC-13/AC-20 structure, which, being rich in fine particles, fosters a more complex fine-scale texture morphology.

This analysis underscores the significant impact of aggregate size and distribution within the upper layer's structure on the textural properties of the pavement interface. Larger aggregates found in OGFC-13 and SMA-13 contribute to deeper but less densely distributed furrows, whereas the finer aggregates prevalent in AC-13/AC-20 lead to a denser, finer-textured surface. These insights not only affirm the relationship between structural composition and interface texture but also highlight the complex balance between furrow depth and density in determining overall pavement texture characteristics.

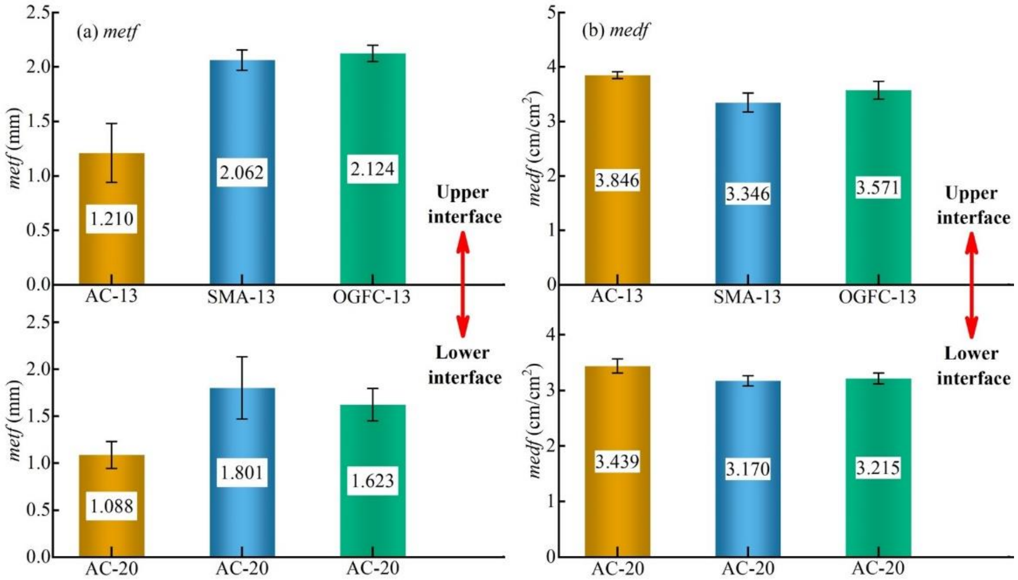

Figure 9. Results of furrow characteristics of interlayer of bi-layered asphalt structures.

4.2. Interlocking effects

The bonding between the upper and lower layers to form a monolithic structure involves more than just the contribution of the tack coat; it also significantly depends on the morphological interactions between the upper and lower interlayer surfaces. Given that the lower layer is laid first, with the upper layer placed subsequently during pavement layer construction, the aggregates from the upper layer tend to embed into the lower layer. This embedding facilitates a mechanical interlock with the aggregates of the lower layer, culminating in the creation of an interlocking state.

This process of interlayer bonding is critical, as it not only enhances the structural integrity of the pavement but also contributes to its durability by improving load distribution and resistance to deformation. The effective interlocking of aggregates across the layers serves as a fundamental mechanism in achieving a robust and resilient pavement structure, underscoring the importance of considering both adhesive and morphological factors in interlayer design and construction.

The analyses conducted thus far reveal that variations in aggregate ratios across different asphalt structures result in distinct interface morphologies, subsequently influencing the nature of interlocking effects. To quantitatively assess these effects, a detailed analysis of the interlayer locking states for each structural configuration was conducted. An interlocking coefficient has been introduced as a quantitative measure to characterize the efficacy of interlocking, with both the methodology for determining this coefficient and the resultant interlocking states depicted in Figure 10.

The calculated interlocking coefficients, which serve as a numerical representation of the interlocking effect, are presented in Table 4, illustrating how differences in aggregate composition and distribution affect the mechanical interlock between pavement layers.

Table 4 reveals a distinct hierarchy in the interlocking coefficients among the studied pavement structures, with AC-13/AC-20 exhibiting the highest coefficient, followed by SMA-13/AC-20, and OGFC-13/AC-20 presenting the lowest value. This variation underscores the impact of differing aggregate compositions and structures on the interlocking effects, as illustrated in Figure 11. In scenarios where AC-20 serves as the uniform lower structure, the finer particle composition of AC-13 facilitates a more comprehensive embedding into the lower layer, thereby achieving a superior interlocking effect. Conversely, the larger aggregate sizes inherent in OGFC-13 and SMA-13 challenge the full integration of the upper layer with the lower layer, diminishing the effectiveness of the interlock.

Particularly notable is the OGFC-13 structure, characterized by its pronounced voids, which contribute to a markedly rough texture on the upper surface. However, these void characteristics complicate the achievement of a tight embedment with the AC-20 lower structure, limiting the interlayer bonding effectiveness. This observation aligns with findings from previous studies (Xu et al. 2023, Chen and Huang 2010), highlighting the crucial role of aggregate size and texture in influencing mechanical interlocking.

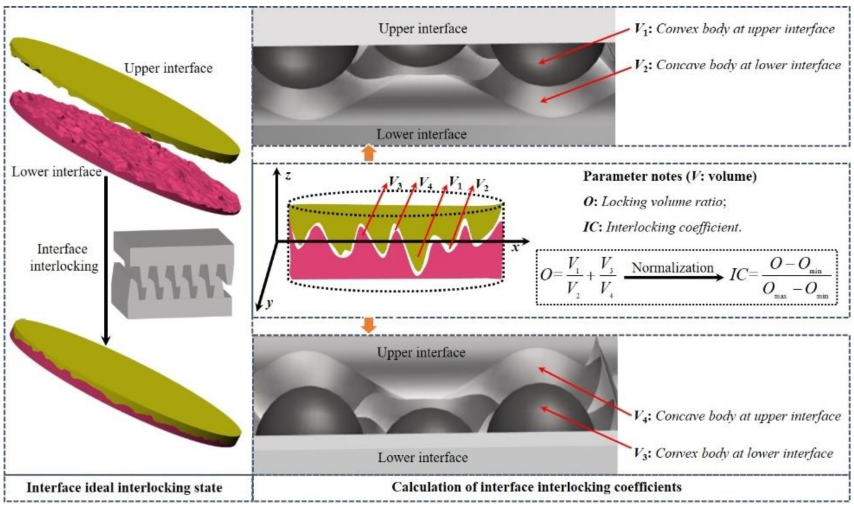

Figure 10. Interlocking states and interlocking coefficients calculation.

Table 4. Results of interlocking coefficient for each structure.

Structure type	AC-13/AC-20	SMA-13/AC-20	OGFC-13/AC-20
IC	0.985	0.801	0.690

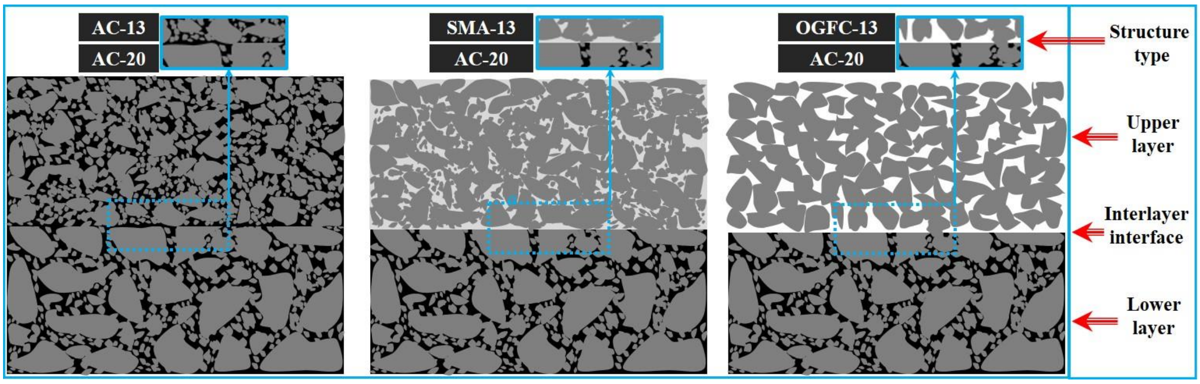

Figure 11. schematic diagram of interlocking effect formed by different upper and lower structures.

4.3. Correlation between morphology parameters and interlocking coefficient

The previous analysis has indicated that there is an obvious correlation between interlocking and interlayer surface morphology. To further clarify and quantify this relationship, the gray correlation method as a robust analytical tool was employed. By employing this approach, it was aimed to reveal the complex interactions between the physical texture of the interlayer surfaces and their capacity to interlock effectively.

Gray correlation analysis serves as a pivotal method in decision-making processes, offering insights into the correlation strengths between a parent series of data and various characteristic series. This methodology is distinguished by its flexibility, as it does not stipulate a minimum sample size nor does it necessitate a predefined pattern within the data sets. Notably, the quantitative results derived from gray correlation analysis are generally in alignment with qualitative assessments, underscoring its efficacy in both fields of analysis (Fen et al. 2011, Dong et al. 2013). The procedure for conducting gray correlation analysis is systematically divided into four essential steps:

(1) Determination of the parent series and characteristic series:

The parent series is the data series reflecting the characteristics of the system behavior, and its calculation formula is shown in Equation (1). The characteristic series is the set of factors affecting the system behavior, and its calculation formula is shown in Equation (2).

$$Y = Y(k) \,|\, k = 1, 2 \ldots n \tag{1}$$

$$X_i = X_i(k) \,|\, k = 1, 2 \ldots n, i = 1, 2 \ldots, m \tag{2}$$

where $Y(k)$ is the parent series; $X_i(k)$ is the characteristic series; *i* is the number of characteristics (the number of influencing factors); and *n* and *m* are the series dimensions.

(2) Standardization of data:

Given the potential variability in data magnitude and dimensions, standardization is crucial to ensure that all data points are comparable, facilitating a more accurate correlation analysis.

(3) Calculation of the gray correlation coefficient:

This step entails computing the correlation coefficients between the parent and characteristic series. These coefficients quantify the degree of association, highlighting similarities and divergences in patterns or trends.

Let the parent sequence be $Y{=}Y(k)$, and the characteristic sequence be $X_i{=}X_i(k)$, then the minimum and maximum differences between the parent sequence and the characteristic sequence are calculated by using Equations (3) and (4), and on this basis, the correlation coefficient between $Y(k)$ and $X_i(k)$ is calculated as shown in Equation (5).

$$a = \min\left|Y(k) - X_i(k)\right| \quad (3)$$

$$b = \max\left|Y(k) - X_i(k)\right| \quad (4)$$

$$\xi_i(k) = \frac{a + \rho b}{\left|Y(k) - X_i(k)\right| + \rho b} \quad (5)$$

where a is the minimum difference between the parent series and the characteristic series; b is the maximum difference between the parent series and the characteristic series; ρ is the resolution coefficient, usually taken as 0.5; and $\xi_i(k)$ is the correlation coefficient.

(4) Analysis and interpretation of results:

The final step involves a comprehensive examination of the correlation coefficients to discern the nature and strength of relationships between the data series, leading to informed conclusions and decision-making insights.

In order to compare the correlation degree between the characteristic series and the parent series as a whole, the correlation coefficients of each point on the series curve are pooled into one value, i.e. the average value is obtained as the numerical representation of the correlation degree between $Y(k)$ and $X_i(k)$, and it is calculated as shown in Equation (6). Finally, the calculated correlation degree values are ranked according to the calculated correlation degree values to find out the magnitude of the influence of factors in the characteristic sequence and evaluate it.

$$R_i = \frac{\sum_{k=1}^{n} \xi_i(k)}{n}, k = 1, 2..., n \quad (6)$$

where R_i is the degree of correlation between $Y(k)$ and $X_i(k)$.

In this analysis, the interlocking coefficient (*IC*) is designated as the parent series, while the various interface morphology parameters serve as the characteristic series. The correlation degree between each morphology parameter and the *IC* was calculated following Equations (1) to (6), as illustrated in Figure 12. Analysis of the data presented in Figure 12 reveals that, with the exception of *Ssk*, all other morphology parameters exhibit a significant correlation with the *IC*. This finding underscores the considerable impact of interface morphology characteristics on the interlocking effect.

The substantial correlation between most morphology parameters and the *IC* highlights the critical role of surface texture and geometry in enhancing the mechanical interlock between pavement layers. This relationship suggests that optimizing these morphological characteristics can significantly contribute to the overall stability and durability of pavement structures by improving the efficacy of interlayer bonding.

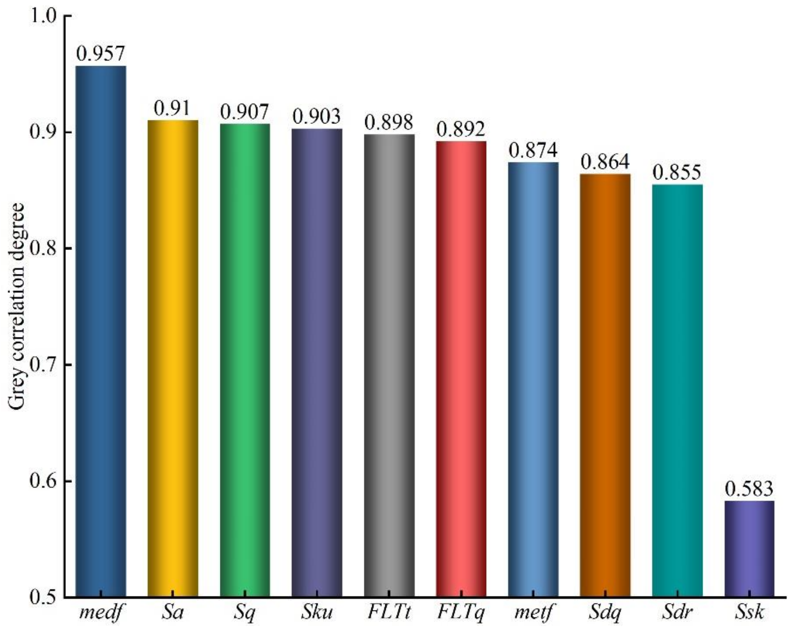

Figure 12. Correlation degree between interface morphology characteristics and interlocking coefficient.

To further explore the relationship between interface morphology parameters and interlocking coefficient, the following 2 steps were taken:

(1) Application of the Pearson correlation test: This statistical approach was employed to examine the correlation and potential substitutability among the morphological parameters. The Pearson correlation test, a widely recognized method for assessing the linear relationship between continuous variables, allowed us

to pinpoint the morphological characteristics most indicative of effective interlocking. The results of this analysis are visually summarized as a correlation matrix heatmap presented in Figure 13, which maps the strength and direction of correlations between parameters, thereby highlighting those with the most pronounced impact on characterizing the interface morphology.

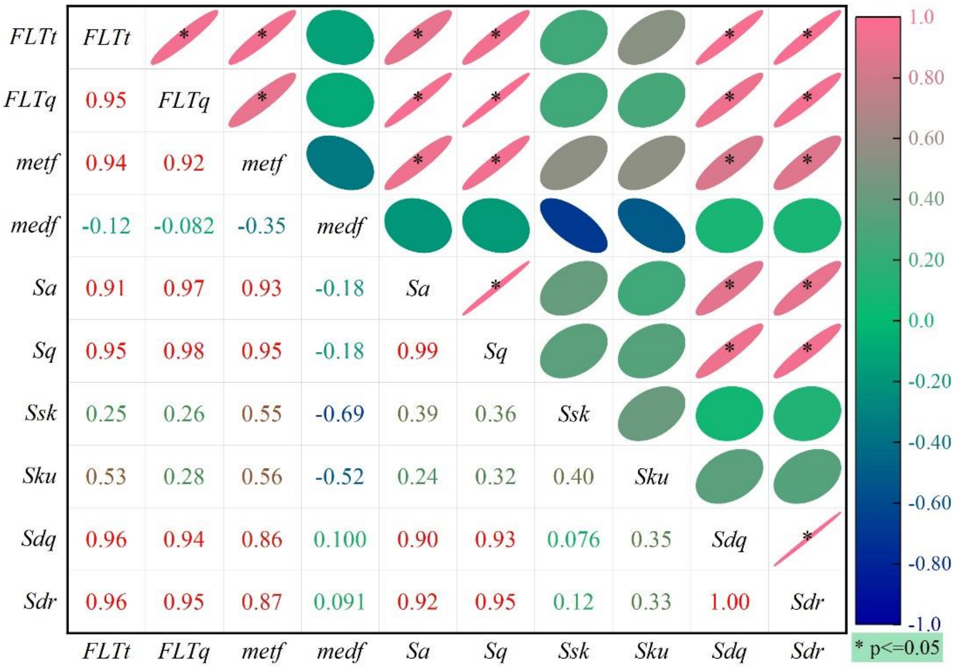

Figure 13. Correlation matrix heatmap of the parameters characterizing the interface morphology.

Analysis of the correlations presented in Figure 13 reveals differentiated relationships among the interface morphology parameters. Notably, *medf* is characterized by a minimal, and in most cases negative, correlation with other parameters, indicating its distinct behavior. Similarly, *Ssk* and *Sku* display weak correlations with the majority of parameters, underscoring their unique contributions to the interface morphology. In contrast, *Sa* and *Sq* are highly correlated with each other and show strong positive correlations with the rest of the parameters, suggesting their potential interchangeability in representing surface roughness. In addition, *Sdq* and *Sdr* exhibit a high degree of correlation, indicating that one could serve as a proxy for the other. *FLTq* is also observed to have a strong positive correlation with both *Sa* and *Sq*, further validating the interconnectedness of these parameters.

Taking into account the correlation strengths with the interlocking coefficient (*IC*) as shown in Figure 12, *Ssk* is deemed less relevant due to its minimal correlation. Among parameters with substitutable roles, the one exhibiting the strongest correlation with *IC* is retained for further analysis. Consequently, the selected parameters for characterizing interface morphology include *FLTt*, *metf*, *medf*, *Sa*, *Sku*, and *Sdq*. This selection strategy prioritizes parameters that not only reflect critical aspects of interface morphology but also have a demonstrable impact on the interlocking effect, thus offering a refined lens through which to assess and enhance interlayer bonding.

(2) Upon careful examination of Figures 7 and 9, it is observed that the parameters *Ssk*, *Sku*, *Sdq*, Sdr, and *metf* display varied trends of change between the upper and lower interlayer surfaces. This variability introduces complexities in defining a consistent correlation function to effectively capture the nuances of the interlocking effect. Due to these observed inconsistencies and the challenge they pose in establishing a clear, unified model of interlayer interaction, these parameters were ultimately excluded from further consideration in the correlation analysis.

As a result, *FLTt*, *medf*, and *Sa* have been identified as the key morphological parameters for the study, each representing a distinct aspect of interface morphology: *FLTt* for interface flatness, *medf* for texture furrow density, and *Sa* for texture roughness. The selection of these parameters is strategic, focusing on those that not only exhibit consistent patterns of behavior across different interfaces but also hold significant potential in explaining the relationship between interface morphology and the interlocking effect. This refined approach aims to streamline the analysis, directing attention to the most impactful aspects of interface morphology on interlayer bonding.

4.4. Relationship between interlocking effect and interlayer shear strength

The interlocking effect is a critical determinant of interlayer shear strength within pavement structures, as highlighted by (Zareiyan and Khoshnevis 2017). Analysis of the interlayer shear strength test results for double-layered asphalt systems, as shown in Figure 14, reveals that the AC-13/AC-20 structure exhibits the highest interlayer shear strength. This is followed by SMA-13/AC-20, while OGFC-13/AC-20 shows the lowest shear strength. Such variations underscore the influence of upper layer composition on the interface contact effects, particularly the mechanical interlocking between the layers.

A review of the interlocking coefficients detailed in Table 4 establishes a positive correlation with interlayer shear strength. Specifically, a higher interlocking coefficient signifies a more pronounced interlocking effect between the upper and lower layers. This enhanced interlocking, in turn, contributes to increased interlayer friction, resulting in elevated shear strength. This relationship suggests that optimizing the interlocking characteristics of the interlayer can significantly contribute to the overall structural integrity and durability of pavement layers by enhancing their capacity to resist shear forces.

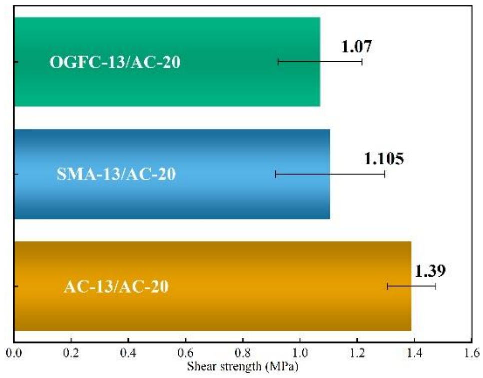

Figure 14. Interlayer shear strength for different asphalt structures.

Based on the statistical analysis, a functional relationship between interlayer shear strength and the interlocking coefficient was acquired, as shown in Equation (7). This equation reveals a substantial correlation between the two variables, underscored by an R^2 value of 0.891. Such a high R^2 value attests to the robustness and reliability of the fitted relationship, affirming that the interlayer shear strength can be reliably predicted based on the interlocking coefficient.

The validation of the predictive model was carried out by comparing its estimations against the actual measured interlayer shear strengths, as displayed in Figure 15. The results demonstrate that the model performs with remarkable accuracy, substantiating its utility in reliably forecasting interlayer shear strength across studied pavement structures.

The efficacy of this predictive model was further quantified through the R-squared statistic, serving as a measure of the model's ability to capture the variance in measured data. Notably, the model predicated on the interlocking coefficient achieves an R^2 value of 0.896, signifying a strong and robust correlation between predicted and observed values.

$$\tau = 0.204 + 1.193IC,\ R^2 = 0.891 \quad (7)$$

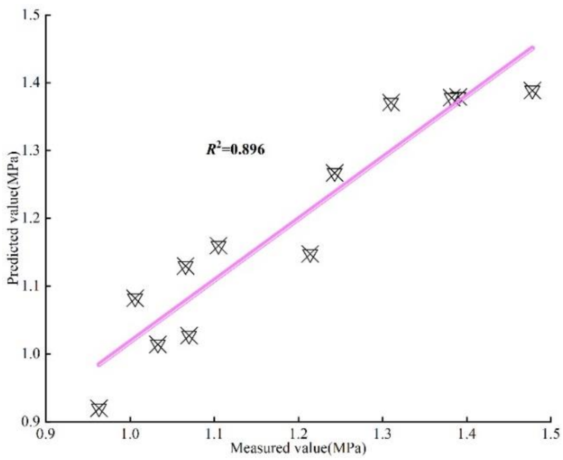

Figure 15. The relationship between measured and predicted values of interlayer shear strength based on *IC*.

The findings from the discussed analysis underscore the pivotal role of the interlocking effect in defining interlayer shear strength. Furthermore, it has been established that surface characteristics of the interlayer significantly influence this interlocking effect. To quantitatively assess the impact of the identified interface morphology parameters on interlayer shear strength, a statistical analysis of variance (ANOVA) was employed. The results of this analysis are detailed in Table 5, where a significance level of 0.05 was applied, reflecting a confidence level of 95%.

The analysis revealed that the *p*-value associated with the interface morphology parameters was significantly below the 0.05 threshold. This finding unequivocally indicates that the variations in interface morphology exert a statistically significant influence on the interlayer shear strength.

Table 5. One-way ANOVA results for interlayer shear strength based on surface characteristics.

Variance source	SS	DF	MS	*F*-value	*P*-value
Between-group	0.129	2	0.065	4.042	0.039
Within – group	0.240	15	0.016		
Total	0.370	17			

Note: SS = sum of squares; DF = degrees of freedom; MS = mean square, which is the SS divided by DF; *F*-value = ratio of mean squares, which is used to determine the *P*-value.

4.5. Interlayer shear strength prediction model

The comprehensive analysis conducted thus far has highlighted the crucial influence of interface morphology on the interlocking effect between upper and lower interlayer surfaces, which, in turn, significantly impacts interlayer shear strength. Recognizing the complexity and the computational demands involved in directly modeling and calculating the interlocking effect, a streamlined approach was proposed. This approach entails utilizing the interlocking effect as an intermediary variable, thereby facilitating a more straightforward evaluation of interlayer shear bonding strength.

A correlation function was developed to describe the relationship between interface morphology characteristics and interlayer shear strength. This method allows for the direct assessment of interlayer shear strength by analyzing interface morphology characteristics, avoiding the need for complex calculations related to the interlocking effect. Following the careful selection of representative parameters to incorporate the interface morphology, the following Equation (8) was developed to articulate the correlation function between these selected parameters and interlayer shear strength:

$$\tau = 1.5628 + 0.0835FLTt + 0.2147medf - 2.5793Sa \quad (8)$$

It's crucial to note that, for the practical application of Equation (8), consistency in the source of morphological parameter values is essential. Specifically, all morphological parameters integrated into this equation must be derived exclusively from either the upper or the lower interlayer surfaces, not a combination of both. This uniform approach ensures the reliability and accuracy of the predictive model, as mixing values from different layers could introduce variability that undermines the equation's predictive capability.

Figure 16 showcases that the predictive model achieves an accuracy of 0.745. This level of accuracy, while indicative of a correlation, points towards a modestly robust relationship between the predicted values of interlayer shear strength and the interface morphology characteristics. Such findings imply that, although it is possible to deduce aspects of interlayer shear bonding from the interface morphology, the reliability of these deductions has its limitations. This observation underscores a reality: while interface morphology exerts a considerable influence on the interlocking effect, and the interlocking state, in turn, impacts interlayer shear strength significantly, forging a definitive link between interface morphology characteristics and interlayer shear strength proves to be complex.

This complexity might stem from the model's potential limitations in encompassing all relevant factors or from a complex interplay between interface morphology and the interlocking effect that the model fails to fully capture. Consequently, this suggests that for a more accurate and reliable prediction of interlayer shear strength, future models may need to consider a broader range of factors or more deeply explore the interaction between interface morphology and the interlocking effect.

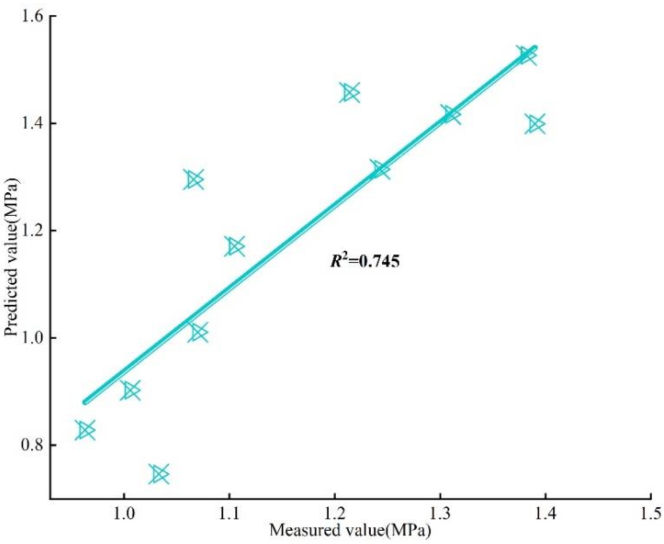

Figure 16. Measured and predicted values of interlayer shear strength based on morphological characteristics.

5. Conclusions

This study pioneered the integration of non-destructive interlayer separation techniques with 3D laser scanning to reveal the complex interface morphology of double-layer asphalt systems, paving the way for an innovative assessment of interlayer bonding performance. Through careful morphological parameter analysis, it was demonstrated that how variations in particle size and upper layer compositions fundamentally alter interface characteristics, impacting the interlocking contribution and, consequently, interlayer shear strength. The following conclusions can be drawn from this study:

(1) Influence of particle size and composition: Variations in mineral sizes within the asphalt mix significantly alter interface texture, with the upper layer's composition playing a pivotal role in morphological reshaping, particularly when compared against a consistent AC-20 lower layer.

(2) Morphological characteristics' impact on interlocking: The SMA-13/AC-20 and OGFC-13/AC-20 systems demonstrated pronounced morphological characteristics, influencing the interlocking effect. The developed predictive model, while marking a significant advancement, underscores the complexity of establishing a direct correlation between interface morphology and shear strength.

(3) Predictive model advancements: The formulation of a predictive model for interlayer shear strength, utilizing interlocking characteristics as an intermediary variable, signifies a leap forward in assessing interlayer bonding performance. However, this model's partial reflection of shear bonding characteristics invites further exploration into the multifaceted relationship between interface morphology and interlocking effect.

In essence, this study not only sheds light on the significant role of interface morphology in enhancing interlayer bonding but also highlights the need for continued research to refine the predictive model for broader applicability across varied pavement structures. Future research will focus on expanding the scope of interlayer treatments and exploring diverse asphalt systems to attain a more robust understanding of the interplay between interface morphology and interlayer bond strength.

Author information

First author: Hongzhi He, E-mail address: hhzxz9527@163.com

***Corresponding author:** Changfa Ai，E-mail address**:** cfai@home.swjtu.edu.cn

Declaration of Competing Interest

The authors declare that they have no known competing financial interests or personal relationships that could have appeared to influence the work reported in this paper.

Acknowledgements

This work was supported by the National Natural Science Foundation of China [grant No. 52278462 and No. 51878574], Fundamental Research Funds for the Central Universities, SWJTU [grant No. 2682022CX002], and Sichuan Science and Technology Program [Grant No. 2021JDTD0023].

References

Ai, C., et al. 2022. Investigation of inter-layer bonding property in asphalt pavement based on 3D morphology of reconstructed interface. Construction and Building Materials, 317.

Aver'yanova, I. O., Bogomolov, D. Y. and Poroshin, V. V. 2017. ISO 25178 standard for three-dimensional parametric assessment of surface texture. Russian Engineering Research, 37(6), 513-516.

Canestrari F, F. G., Lu X 2013. Mechanical testing of interlayer bonding in asphalt pavements. Advances in Interlaboratory Testing and Evaluation of Bituminous Materials: State-of-the-Art Report of the RILEM Technical Committee 206-ATB, 303-360.

Čelko, J., Kováč, M. and Kotek, P. 2016. Analysis of the Pavement Surface Texture by 3D Scanner. Transportation Research Procedia, 14, 2994-3003.

Chen, J.-S. and Huang, C.-C. 2010. Effect of Surface Characteristics on Bonding Properties of Bituminous Tack Coat. Transportation Research Record: Journal of the Transportation Research Board, 2180(1), 142-149.

Chen, S., et al. 2022. Reinforcement of interlaminar mechanical properties between rigid and flexible layers of semi-rigid base asphalt pavement using interlayer treatment. International Journal of Pavement Engineering, 1-6.

China, C. o., 2004. Technical specifications for construction of highway asphalt pavements. Beijing: Research Institute of Highway Ministry of Transport.

China, C. o., 2011. Highway Engineering Asphalt and Asphalt Mixture Test Procedure. Beijing: Highway Research Institute Ministry of Transport.

Correia, N. S. and Mugayar, A. N. 2021. Effect of binder rates and geogrid characteristics on the shear bond strength of reinforced asphalt interfaces. Construction and Building Materials, 269.

D'Andrea, A., et al. 2013. Interface Roughness Parameters and Shear Strength. Modern Applied Science, 7(10).

Das, A., et al. 2021. Surface microtexture and wettability analysis of quasi two-dimensional (Ti, Al)N thin films using fractal geometry. Surface and Coatings Technology, 421.

Dong, Y. S., Liu, Q. Q. and Cao, D. W. 2013. Research of Influencing Factor on the Bending Property of Asphalt Mixture Based on Grey Correlation Entropy. Applied Mechanics and Materials, 405-408, 1923-1927.

Fen, Y., et al. 2011. Evaluation of Shear Performance of Flexible Waterproof-adhesive Layer in Concrete

Bridge Pavement Based on Grey Correlation Analysis. Road Materials and Pavement Design, 10(sup1), 349-360.

Ghabchi, R. and Dharmarathna, C. P. 2020. Effect of tack coat emulsion type, application rate, and surface type and texture on early-age interlayer shear strength of pavements in cold regions. International Journal of Pavement Engineering, 23(6), 1881-1896.

Goli, A., et al. 2023. Evaluation of Mechanical Characteristics and Plastic Coating Efficiency in Plastic-Modified Asphalt Mixes. International Journal of Pavement Research and Technology, 16(3), 693-704.

Han, Y., et al. 2021. Effects of design parameters and moisture conditions on interface bond strength between thin friction course (TFC) and underlying asphalt pavements. Construction and Building Materials, 269, 121347.

He, H., et al. 2023. Characterization of Interlayer Bonding Mechanism Based on Interface Morphology in Double-Layered Asphalt Systems. Journal of Materials in Civil Engineering, 35(6).

Hoła, J., et al. 2015. Usefulness of 3D surface roughness parameters for nondestructive evaluation of pull-off adhesion of concrete layers. Construction and Building Materials, 84, 111-120.

Hristov, B. 2018. Influence of Different Interface Properties on the Interlayer Bond Shear Stiffness. IOP Conference Series: Materials Science and Engineering, 365.

Hwang, H.-S., et al. 2022. Investigation of texture effects at interlayer bonding behavior between asphalt concrete (AC) overlay on Portland cement concrete (PCC). Canadian Journal of Civil Engineering, 49(3), 412-419.

Jain, S., Das, A. and Venkatesh, K. S. 2021. Automated and contactless approaches for pavement surface texture measurement and analysis – A review. Construction and Building Materials, 301.

Jaskula, P., et al. 2021. Optimisation and field assessment of poroelastic wearing course bond quality. Road Materials and Pavement Design, 22(sup1), S604-S623.

Kogbara, R. B., et al. 2016. A state-of-the-art review of parameters influencing measurement and modeling of skid resistance of asphalt pavements. Construction and Building Materials, 114, 602-617.

Ktari, R., et al. 2017. Surface roughness: a key parameter in pavement interface design. European Journal of Environmental and Civil Engineering, 21(sup1), 27-42.

Liao, G., Wang, S. and Shi, Q. 2016. Enhancing anti-rutting performance of asphalt pavement by dispersing shear stresses within asphalt layers. Road Materials and Pavement Design, 19(2), 453-469.

Liu, G., et al. 2018. Interlayer shear strength of Roller compacted concrete (RCC) with various interlayer treatments. Construction and Building Materials, 166, 647-656.

Liu, X., et al. 2017. Experimental study on interlayer shear properties of ERS pavement system for long-span steel bridges. Construction and Building Materials, 143, 198-209.

Medeiros Jr, M., et al. 2021. 3D pavement macrotexture parameters from close range photogrammetry. International Journal of Pavement Engineering, 1-15.

Mohamad, M. E., et al. 2015. Friction and cohesion coefficients of composite concrete-to-concrete bond. Cement and Concrete Composites, 56, 1-14.

Nadolny K, K. W. 2014. Analysis of flatness deviations for austenitic stainless steel workpieces after efficient surface machining. Measurement science review, 14(4), 204-212.

Raab, C., 2011. Development of a framework for standardisation of interlayer bond of asphalt pavements. Carleton University.

Raab, C., Abd El Halim, A. O. and Partl, M. N. 2012. Interlayer bond testing using a model material. Construction and Building Materials, 26(1), 190-199.

Ram Kumar B A V, J. H. 2022. Performance of Geogrid Reinforced Asphalt Layers—A Review. Recent Advancements in Civil Engineering: Select Proceedings of ACE 2020, 683-399.

Ren, W., et al. 2018. Research on interlaminar shear properties of bridge deck asphalt pavement on chip-sprinkling cement concrete. Journal of Building Materials, 21(01), 111-116.

Schulz, E., Calandra, I. and Kaiser, T. M. 2013. Feeding ecology and chewing mechanics in hoofed mammals: 3D tribology of enamel wear. Wear, 300(1-2), 169-179.

Sha, A., et al. 2020. Influence of sampling interval and evaluation area on the three-dimensional pavement parameters. Road Materials and Pavement Design, 22(9), 1964-1985.

Solatiyan, E., Bueche, N. and Carter, A. 2021. Laboratory evaluation of interfacial mechanical properties in geogrid-reinforced bituminous layers. Geotextiles and Geomembranes, 49(4), 895-909.

Somé, S. C., et al. 2020. Mechanical characterization of asphalt mixes inter-layer bonding based on reptation theory. Construction and Building Materials, 242.

Song, W., et al. 2015. Factors affecting shear strength between open-graded friction course and underlying layer. Construction and Building Materials, 101, 527-535.

Song, W., et al. 2017. Influence of Interface Characteristics on the Shear Performance between Open-Graded Friction Course and Underlying Layer. Journal of Materials in Civil Engineering, 29(8).

Song, W., et al. 2018. Effects of Asphalt Mixture Type on Asphalt Pavement Interlayer Shear Properties. Journal of Transportation Engineering, Part B: Pavements, 144(2).

Song, W., et al. 2022. Laboratory investigation of the bonding performance between open-graded friction course and underlying layer. Engineering Fracture Mechanics, 265.

Tang, Z., Huang, F. and Peng, H. 2021. Effect of 3D roughness characteristics on bonding behaviors between concrete substrate and asphalt overlay. Construction and Building Materials, 270.

Tashman, L., et al. 2008. Evaluation of construction practices that influence the bond strength at the interface between pavement layers. Journal of Performance of Constructed Facilities, 22(3), 154-161.

White, G. 2016. State of the art: interface shear resistance of asphalt surface layers. International Journal of Pavement Engineering, 18(10), 887-901.

Wruck, B. M., et al. 2022. Impact of Emulsion Type, Application Rate, and Adverse Construction Conditions on Tack Coat Performance. Transportation Research Record: Journal of the Transportation Research Board, 2677(3), 535-550.

Xu, J., et al. 2023. Mesodamage Mechanism of Asphalt Mixtures with Different Structural Types under Frost Heaving of Ice Crystals. Journal of Materials in Civil Engineering, 35(1).

Zareiyan, B. and Khoshnevis, B. 2017. Effects of interlocking on interlayer adhesion and strength of structures in 3D printing of concrete. Automation in Construction, 83, 212-221.

Zhao, H., Cao, J. and Zheng, Y. 2017. Investigation of the interface bonding between concrete slab and asphalt overlay. Road Materials and Pavement Design, 18(sup3), 109-118.